MIXING AND CHEMICAL REACTION IN AN IDEALIZED SWIRL CHAMBER

Omar M. Knio and Aniruddha S. Worlikar
Department of Mechanical Engineering
The Johns Hopkins University
Baltimore, MD 21218-2686

and

Habib N. Najm
Sandia National Laboratories
P.O. Box 969, MS 9051
Livermore, CA 94551

Corresponding Author:

Omar M. Knio
Department of Mechanical Engineering
The Johns Hopkins University
Baltimore, MD 21218-2686
Phone: (410) 516-7736
FAX: (410) 516-7254
email: knio@flame.me.jhu.edu

Paper length (using MS-Word utilities):

a.	Abstract	265 words
b.	Manuscript	2,903 words (Introduction through Conclusions)
c.	Equations	378 words (12 @ 21 words; 3 @ 42)
d.	Nomenclature	273 words (39 lines @ 7 words/line)
e.	Figures	2,000 words-equivalent
Total b-e		5,554

Preferences: Oral Presentation in one of the following sessions: Turbulent Non-Premixed Combustion, or Turbulent Premixed and Partially Premixed Combustion

Submitted to *Twenty-Sixth Symposium (International) on Combustion*
January 1996

MIXING AND CHEMICAL REACTION IN AN IDEALIZED SWIRL CHAMBER

Omar M. Knio and Aniruddha S. Worlikar
Department of Mechanical Engineering
The Johns Hopkins University
Baltimore, MD 21218-2686

and

Habib N. Najm
Sandia National Laboratories
P.O. Box 969, MS 9051
Livermore, CA 94551

ABSTRACT

A vorticity-based, low-Mach-number model for the simulation of combustion in closed chambers is constructed. The numerical scheme is based on a mixed finite-difference pseudo-spectral discretization of the governing equations. Discrete evolution equations are integrated in time using a predictor-corrector scheme, while discrete elliptic systems are inverted with the help of a fast-Poisson solver. The scheme is applied to analyze mixing and combustion in an idealized swirl cavity, which consists of the annular space between a spinning inner cylinder and a stationary outer cylinder. Attention is focused on the effect of partial mixing on the development of the reaction. To this end, we assume that the oxidizer and fuel are initially separated by a thin mixed region, and carefully control mixing levels by varying the duration of the swirl-driven mixing period. The mixture is then ignited along the boundary of the inner cylinder. When pre-mixing is complete, an axisymmetric flame front is established, and the reactants are consumed as the front propagates radially outwards. When the charge is partially mixed, combustion in the early stages predominantly occurs within a non-uniform premixed front. As this non-uniform front approaches the outer cylinder, a transition to a distributed combustion regime occurs. Following the transition, the remaining fuel burns at a slow rate within non-premixed flames which wrap around the inner cylinder. Results show that the mixing time has substantial effects on the pressure rise within the cavity and on the evolution of the burnt fraction, and that these effects become more pronounced as the Damköhler number increases.

INTRODUCTION

In a wide range of applications, swirling velocity fields are exploited as means to enhance the performance of combustion systems. For example, rotating flow fields have been effectively used to improve flammability limits of premixed flames, both in counterflow (*e.g.* [1]) and stagnation-point flow (*e.g.* [2]) configurations. Swirling motions are also employed to drastically alter the features of the reacting field, and/or stabilize the combustion process; swirl-stabilized combustors (*e.g.* [3]) are prominent examples of such applications. In yet another application regime, swirl is actively induced in order to promote mixing and reaction rates; gas turbines, furnaces, and IC engines (*e.g.* [4-6]) typically involve vigorous swirling motions.

When primarily used to promote mixing and combustion, the "design" of swirling motion is generally faced with two, often conflicting, requirements. On one hand, it is desirable to have high swirl so as to achieve adequate mixing between oxidizer and fuel; on the other, the strain rates associated with the imposed swirl must not be so large as to cause extinction or quenching of the reaction. Thus, it is possible that the selected flow conditions result in a highly non-uniform mixture, and that premixed and non-premixed combustion regimes simultaneously prevail. Such situations may result in complex combustion processes; the generation of "triple-flames" [7] exemplifies one aspect of the impact of mixture non-uniformity.

This paper relies on a simplified model problem to observe and analyze flow phenomena which are relevant to partially-mixed, swirl-driven, reacting flows. As shown in Fig. 1, we consider an idealized swirl cavity which consists of the annular region between concentric cylinders. The swirling motion within the cavity is solely due to the constant spinning of the inner cylinder; the outer cylinder remains fixed. Initially, the oxidizer and fuel are separated by a thin mixed zone which extends in the radial direction. The oxidizer and fuel are allowed to mix in the swirling field for a predetermined period before the mixture is ignited. The amount of mixing is controlled by varying the (swirl-enhanced) mixing time. Different initial conditions for combustion are thus produced, and the impact of partial mixing on the development of the reaction and pressure rise is analyzed numerically using a low-Mach-number combustion model. The computations are performed using a new numerical scheme whose construction is summarized below.

FORMULATION AND NUMERICAL SCHEMES

The physical model used in the present study is similar to that in Ref. [8]. Here, we assume that the flow is 2D, and that chemical species obey the perfect gas law, and have equal molecular weight, equal and constant values of dynamic viscosity, thermal conductivity, and mass diffusivity. The low-Mach-number approximation of the governing equations is used [9-11], allowing us to ignore acoustic wave propagation and to decompose the pressure field into a spatially-uniform thermodynamic component, $P(t)$, and hydrodynamic component, $p(\mathbf{x},t)$. In

addition, a simplified chemical model is adopted which assumes a single-step irreversible Arrhenius-rate reaction. We rely on a vorticity-based formulation of the governing equations which, under the above assumptions, reduce to [8]:

Conservation of Mass
$$\nabla \bullet \mathbf{u} = -\frac{1}{\gamma P}\frac{dP}{dt} + \frac{1}{P\,\mathrm{Pr}\,\mathrm{Re}}\nabla^2 T - Q\frac{\dot{w}_f}{P} \tag{1}$$

Vorticity Transport
$$\frac{\partial \omega}{\partial t} = \nabla \times (\mathbf{u} \times \omega) + \frac{1}{\rho\,\mathrm{Re}}\nabla^2 \omega - \frac{\nabla \rho}{\rho} \times \frac{D\mathbf{u}}{Dt} \tag{2}$$

Energy
$$\frac{\partial T}{\partial t} = -\mathbf{u} \bullet \nabla T + \frac{1}{\rho}\frac{\gamma - 1}{\gamma}\frac{dP}{dt} + \frac{1}{\rho\,\mathrm{Pr}\,\mathrm{Re}}\nabla^2 T - Q\frac{\dot{w}_f}{\rho} \tag{3}$$

Species
$$\frac{\partial C_i}{\partial t} = -\mathbf{u} \bullet \nabla C_i + \frac{1}{\rho Le\,\mathrm{Pr}\,\mathrm{Re}}\nabla \bullet (\rho \nabla C_i) + \frac{\dot{w}_i}{\rho} \tag{4}$$

State
$$P = \rho T \tag{5}$$

Chemical reaction
$$\phi^* \chi_f + \chi_o \rightarrow \chi_p \tag{6}$$

Arrhenius Kinetics
$$\frac{\dot{w}_f}{\rho} = \phi_f \frac{\dot{w}_o}{\rho} = -\rho Da C_f C_o \exp(-\frac{T_a}{T}) \tag{7}$$

Following Najm [11], we combine the global mass conservation constraint with the energy equation to obtain the pressure evolution equation:

$$\frac{dP}{dt} = \int_v \frac{1}{T}\left(\frac{\nabla^2 T}{\mathrm{Pr}\,\mathrm{Re}} - Q\dot{w}_f - \rho \mathbf{u} \bullet \nabla T\right) d\mathbf{x} \Big/ \int_v \frac{1}{\gamma T} d\mathbf{x} \tag{8}$$

The governing equations are solved numerically using a "semi-implicit" predictor-corrector approach. Specifically, we use the third-order Adams-Bashforth scheme to obtain intermediate estimates for species, temperature, thermodynamic pressure, and vorticity

$$\begin{bmatrix} C_i \\ T \\ P \\ \omega \end{bmatrix}^* = \begin{bmatrix} C_i \\ T \\ P \\ \omega \end{bmatrix}^n + \frac{23\Delta t}{12}\begin{bmatrix} S_{c_i} \\ S_T \\ S_P \\ S_\omega \end{bmatrix}^n - \frac{16\Delta t}{12}\begin{bmatrix} S_{c_i} \\ S_T \\ S_P \\ S_\omega \end{bmatrix}^{n-1} + \frac{5\Delta t}{12}\begin{bmatrix} S_{c_i} \\ S_T \\ S_P \\ S_\omega \end{bmatrix}^{n-2} \tag{9}$$

and then update the intermediate values using Crank-Nicolson differencing:

$$\begin{bmatrix} C_i \\ T \\ P \\ \omega \end{bmatrix}^{n+1} = \begin{bmatrix} C_i \\ T \\ P \\ \omega \end{bmatrix}^n + \frac{\Delta t}{2}\begin{bmatrix} S_{c_i} \\ S_T \\ S_P \\ S_\omega \end{bmatrix}^* + \frac{\Delta t}{2}\begin{bmatrix} S_{c_i} \\ S_T \\ S_P \\ S_\omega \end{bmatrix}^n \tag{10}$$

Here, S_{c_i}, S_T, S_P and S_ω denote the species, temperature, pressure and vorticity source terms, given by the right-hand sides of Eqs. (4), (3), (8) and (2) respectively.

Spatial discretization of field quantities is performed in the polar (r,θ) coordinate system and is based on a mixed pseudo-spectral (θ-direction) finite-difference (r-direction) approach. Radial derivatives are approximated using second-order centered differences while azimuthal derivatives are approximated using spectral collocation derivatives. Uniform grids are used both in the θ and r directions.

At the end of each fractional step, the velocity field is reconstructed based on the updated vorticity and divergence field by inverting the following Poisson equation [12]:

$$\nabla^2\mathbf{u} = \nabla(\nabla\bullet\mathbf{u}) - \nabla\times\omega \tag{11}$$

Here, we observe that the solution of Eq. (11) would be straightforward if the vorticity field at the new time level were known, which would be the case if boundary values of vorticity were known. Thus, the problem reduces to specifying appropriate vorticity boundary conditions. To do so, one adequate approach consists of enforcing the definition of vorticity at the boundary of the computational domain, ∂D, *i.e.* imposing:

$$\nabla\times\mathbf{u}\big|_{\partial D} = \omega\big|_{\partial D} \tag{12}$$

As shown by Daube [12], the solution of Eqs. (11-12) is more efficiently performed if one exploits the linearity of the system through boundary Green's functions. Briefly, once the vorticity distribution at internal points is determined, Eq. (11) is inverted by assuming a vanishing vorticity distribution at the boundary. This yields an intermediate velocity field $\tilde{\mathbf{u}}$. Next, we let:

$$\mathbf{u} = \tilde{\mathbf{u}} + \sum_{l=1}^{2}\sum_{k=1}^{N_\theta}\lambda_{k,l}\mathbf{u}'_{k,l} \quad \text{and} \quad \omega\big|_{\Gamma_l} = \sum_{k=1}^{N_\theta}\lambda_{k,l}\exp(ik\theta) \tag{13}$$

where N_θ is the number of boundary points along surfaces Γ_l, $l=1,2$, and $\mathbf{u}'_k$ are solutions to the following elementary problems:

$$\begin{aligned}&\nabla^2\mathbf{u}'_{k,l} = -\nabla\times\omega'_{k,l}\\ &\mathbf{u}'_{k,l}\big|_{\Gamma_l} = 0 \quad l=1,2\end{aligned} \quad \text{with} \quad \omega'_{k,l} = \begin{cases}\exp(ik\theta) & x\in\Gamma_l\\ 0 & \text{otherwise}\end{cases} \tag{14}$$

The unknown coefficients $\lambda_{k,l}$ are determined so that Eq. (12) is satisfied. Taking advantage of the spectral representation in the θ-direction, this requirement is transformed into N_θ decoupled 2x2 systems of linear equations. For modes $k\neq 0$, the corresponding influence matrices are nonsingular, and their inverse are determined in a pre-processing step. The mean vorticity values along each boundary (i.e. the coefficients of the zeroth mode) are determined directly from the force balance along solid boundaries [13]. Steady velocity boundary conditions together with continuity of the pressure along the θ-direction imply a zero net boundary vorticity flux:

$$\int_{\Gamma_l} \frac{\partial \omega}{\partial n} d\mathcal{A} = \frac{\partial \omega'_{0,l}}{\partial r} = 0 \qquad (15)$$

Enforcing Eq. (15) yields the desired values of the coefficients $\lambda_{0,l}$, $l = 1,2$.

RESULTS AND DISCUSSION

The computational model summarized above is applied to analyze mixing and reaction in the geometry shown in Fig. 1. The following conventions are used in the definition of dimensionless groups and in the discussion of computed results. The initial temperature and thermodynamic pressure are used as reference thermodynamic quantities. Meanwhile, the radius of the outer cylinder and the velocity of the inner cylinder are chosen as reference length and velocity scales, respectively. Thus, the spinning cycle of the inner cylinder has normalized period 0.4π. In order to restrict the analysis, most of the dimensionless groups are kept constant. Specifically, in all cases considered, the Reynolds number $\mathrm{Re} = 1000$, the specific heat ratio $\gamma = 1.4$, while unity Lewis and Prandtl numbers are assumed. The stoichiometry of the reaction $\phi = 1$, while the normalized activation temperature and heat release parameter are held at $T_a = 20$ and $Q = 6$, respectively. In all cases, the computations are performed on a fine grid with $N_r = 256$ finite-difference points in the $r-$direction and $N_\theta = 256$ collocation points in the $\theta-$direction.

As mentioned in the introduction, mixing is controlled by varying the "mixing" (or ignition) time. To speed-up the computations, the vorticity field is assumed initially uniform. Thus, oxidizer and fuel mix under the action of the corresponding (steady) swirl. During the mixing time, the reaction source terms are set to zero, *i.e.* the oxidizer and fuel are not allowed to react. The reaction is initialized by discontinuously raising the temperature of the inner cylinder to the adiabatic flame temperature at the initial pressure, $T_{f,0} \approx 1 + Q/2$ (Fig. 1). Below, we analyze the impact of varying the "ignition" time, t_{ig}, on the subsequent development of the reaction. The analysis is conducted for two values of the Damköhler number, $Da = 5000$ and $Da = 10000$. Note that our definition of Damköhler number stems from normalization of the governing equations; it does not account for activation energy and thus does not immediately reflect the ratio of flow to flame time scales. As will be evident later, for the present choice of dimensionless groups, the characteristic flow time scale is comparable to the flame propagation time scale.

Swirl-Enhanced Mixing

Mixing is quantified by plotting the evolution of a mixed-fraction index, PM. Obviously, since oxidizer and fuel are initially separated by a thin mixed region, the corresponding PM is small. In the present computations, $PM = 8.5\%$ at $t = 0$. Also note that for well-premixed conditions $C_F = C_O = 1/2$ so that $PM = 1$. Thus, PM provides a simple and attractive measure for characterizing "pre-mixing" levels.

The evolution of PM during the first 24 cycles is depicted in Fig. 2. The latter shows that PM rises rapidly during the early stages, and very slowly for $t > 6\pi$. Examination of the fuel and oxidizer concentrations (not shown) indicates that the behavior of PM is associated with vigorous mixing at inner radial stations and slow mixing at the outer stations. Thus, under the influence of the swirling flow, a well-mixed region forms which essentially consists of an annulus whose inner boundary coincides with the inner cylinder while its outer boundary expands radially outwards. As the outer boundary of the mixed region approaches the stationary outer cylinder, mixing rates decrease rapidly since the remaining (diametrically-opposed) "pockets" of oxidizer and fuel are separated by a large distance (see Figs. 4 and 5 below).

In order to observe the effects of incomplete mixing, we consider mixtures with $PM = 8.5\%$, $PM = 50\%$ and $PM = 90\%$ which, as shown in Fig. 2, are characterized by ignition times $t_{ig} = 0$, $t_{ig} \approx 2\pi$, and $t_{ig} \approx 15\pi/2$, respectively. Predictions for well-premixed conditions, $PM = 100\%$, are also obtained and used in the analysis.

Flame Structure: Premixed Conditions

When well-premixed conditions initially prevail, the flow field remains axisymmetric during the entire duration of the simulation. In this case the swirl has little impact on the development of the reaction, which thus bears strong resemblance to combustion in an initially-quiescent mixture. The combustion process can be divided into two stages: (a) an "ignition delay", during which the charge is rapidly heated in the neighborhood of the spark and a premixed front is established, and (b) propagation of the resulting front outwards in the radial direction. These phenomena can be clearly observed in Fig. 3, which shows radial profiles of burning rate and temperature for a premixed flame with $Da = 10000$.

Figure 3 shows that the flame structure and burning rate change dramatically as the flame moves outwards. In particular, compression of the reactants ahead of the flame is accompanied by an appreciable thinning of the front, and a substantial increase in the peak fuel burning rate. This is indicative of an increase in the burning (or consumption) speed, but this effect cannot be simply extracted from Fig. 3 since the motion of the front depends, in particular, on flame stretch and position [14].

Figure 3 also indicates that the temperature of the reactants increases uniformly during the combustion process. Meanwhile, temperature stratification occurs within the burned zone, where "super-adiabatic" conditions are observed [11]. Also note that the simplified temperature boundary condition used to model the spark results in heat deposition into the mixture in the early stages of combustion. At late stages, however, the model results in heat losses because of the fixed temperature boundary condition.

Results obtained for a premixed flame with $Da = 5000$ reveal some quantitative differences from predictions for $Da = 10000$. In particular, as the Damköhler number is reduced, the thickness of the front increases and the burning speed decreases [14]. However, all the qualitative trends for $Da = 10000$ are observed. Premixed flame results with $Da = 5000$ are thus omitted.

Reaction Structure: Partially-Mixed Conditions

Development of the reaction in the partially-mixed charge differs significantly from the premixed case. We find that the differences are more pronounced when the mixed-fraction index at the time the spark is applied is smaller. We also find that the mechanisms responsible for these differences act similarly in all cases considered. Thus, for brevity, we restrict the discussion to the case with $Da = 10000$ and $t_{ig} = 0$.

Figure 4 shows that in the early stages following ignition, a "flame front" is established in a similar fashion to the premixed case. This result is not surprising since, as noted earlier, vigorous mixing occurs in the immediate neighborhood of the inner spinning cylinder, leading to the establishment of a mixed zone. However, unlike the premixed case, the field is no longer axisymmetric, as substantial variations in the azimuthal direction are detected (Fig. 4a).

Once it is established, the flame front propagates outwards in the radial direction (Fig. 4b). This propagation phase bears strong resemblance to the premixed case, at least until the flame approaches the (stationary) outer boundary. Figure 4c shows that, as the front moves into the outer region where mixing is highly non-uniform, azimuthal variations in burning rates become larger. As shown in Fig. 4d, this is followed by a sudden transition from a regime where combustion predominantly occurs within a front to a predominantly distributed burning regime.

To gain additional insight into this phenomenon, Fig. 5 shows the contours of fuel concentration, oxidizer concentration, products and vorticity which correspond to Fig. 4d. Figure 5 shows that at $t = 6\pi$ combustion occurs in premixed and non-premixed modes simultaneously. The fuel and oxidizer concentration contours show that the regions surrounding the East-West poles of the outer cylinder are well-mixed. The presence of these well-mixed "pockets" is not surprising because the thin mixed zone which is present at the start of the computations extends all the way to the *stationary* outer boundary. Combustion in these pockets occurs primarily in the form of a premixed flame whose shape is obviously affected by the swirling motion. However, the burning rates within these "pockets" are significantly smaller than those occurring within the thin arms which wrap around the inner cylinder (Fig. 4d). Figure 5 shows that the latter structures lie between regions of high oxidizer concentration and high fuel concentration. Thus, combustion within the thin arms occurs primarily in the form of a non-premixed flame.

Finally, we note that the propagation of the flame within the non-uniform mixture leads to, and is affected by, appreciable changes in the structure of the (initially uniform) vorticity field (*e.g.*

Fig. 5b). Detailed examination of the results (not shown) reveals that for the present set-up changes in the vorticity field are more pronounced when azimuthal variations in the burning rate are more important, *i.e.* when the ignition time is small.

Effects of Partial Mixing on Burning and Pressure Rise

To quantify the impact of the mixing time on combustion, Fig. 6 shows the evolution of the thermodynamic pressure and the burnt fraction for all cases considered. Comparison of different curves in Fig. 6 leads to a number of interesting observations, including:

(1) At early stages, the behavior of the pressure rise and burnt fraction is almost identical for all cases considered. This result is in agreement with our earlier observation that the region surrounding the inner cylinder is rapidly mixed, *i.e.* similar conditions prevail soon after the mixture is sparked.

(2) The curves corresponding to different premixing levels deviate from each other well-before the final stages. At $Da = 10000$, burning and pressure rise occur at a faster rate when the charge is better mixed at the ignition time. This trend is also observed for $Da = 5000$ after $t \sim 4\pi$. At early stages ($0 \le t \le 4\pi$), however, Figs. 6(a,c) show that at $Da = 5000$ the curve for $PM = 8.5\%$ overtakes the other curves. This effect is attributed to an enhancement of the reaction due to deformation of the vorticity field which, as noted above, is stronger when the mixing time is smaller.

(3) It is also interesting to note that deviations between predictions for different premixing levels occur sooner, and their magnitudes are larger for $Da = 10000$ than for $Da = 5000$. This result is also expected since for $Da = 5000$ the burning speed is obviously smaller. Consequently, it takes the flame a longer period to reach the outer stations, during which the charge continues to mix under the influence of the swirl. Thus, the slower ($Da = 5000$) flame encounters a better-mixed charge as it propagates outward, which explains the trends observed in the figure.

(4) As mentioned earlier, the transition to a distributed combustion regime, which occurs at late stages when mixing is not complete, is accompanied by a rapid drop in the rates of burning and pressure rise. Figure 6 clearly shows that, following the transition mentioned above, burning rates drop to very small levels. The pressure curves at these late stages show very small changes in time; in some cases, a small drop is recorded due to heat loss at the inner boundary.

(5) Since changes in pressure are extremely small at the late stages of the simulation, we can use the pressure value at the transition point as an effective measure of the "peak" pressure, at least for cases where a pressure maximum is not reached before the end of the computations. Using this concept of peak-pressure to quantify impact of partial mixing, Fig. 6 shows that the drop in peak-pressure due to incomplete mixing can be as high as 16% at $Da = 5000$, and appreciably larger at

$Da = 10000$. Estimates for the loss in burning efficiency are comparable to those of the "loss" in peak-pressure.

CONCLUSIONS

A low-Mach-number, vorticity-based combustion model is constructed and applied to examine effects of partial mixing in an idealized swirl chamber. In particular, results indicate that incomplete mixing may have a dramatic impact on rates of burning and pressure rise. Significant changes in the structure of the reaction zone(s) are also recorded, especially when a predominantly premixed flame front advances into a poorly mixed region. In the present experiments, incomplete mixing generally leads to a loss in combustion efficiency which, in some cases, exceeds 20%. Losses in burning efficiency generally decrease when initial mixing levels increase, and variations are pronounced as the Damköhler number increases.

NOMENCLATURE

c_p	heat capacity at constant pressure
h_f	enthalpy of reaction per unit mass of fuel
k	thermal conductivity
$\mathbf{n}$	outer normal
p	hydrodynamic pressure
t	time
$\mathbf{u}$	velocity vector
B	pre-exponential factor
C	mass fraction
D	mass diffusivity
Da	Damköhler number ($\equiv \phi_f \tilde{B} \tilde{\rho}_0 / \tilde{W}_f \tilde{\Omega}$)
E	activation energy
Le	Lewis number ($\equiv \tilde{D} \tilde{\rho}_0 \tilde{c}_p / \tilde{k}$)
P	thermodynamic pressure
PM	mixed fraction index ($\equiv 4 \int_{\mathcal{V}} C_F C_O dx \Big/ \mathcal{V}$)
Pr	Prandtl number ($\equiv \tilde{k} / \tilde{\mu}\, \tilde{c}_p$)
Q	heat release parameter ($\equiv -\tilde{h}_f / \tilde{c}_p \tilde{T}_0$)
R	radius
Re	Reynolds number ($\equiv \tilde{\rho}_0 \tilde{\Omega} \tilde{R}_1 \tilde{R}_2 / \tilde{\mu}$)
R_g	gas constant
T	temperature
T_a	normalized activation energy ($\equiv \tilde{E} / \tilde{R}_g \tilde{T}_0$)
$\mathcal{V}$	total volume
W	molecular weight

Subscripts

0	value at $t = 0$
O	oxidizer
F	fuel

Superscripts

~	dimensional quantities

Greek letters

ϕ^*	molal stoichiometry
ϕ	mass stoichiometry
γ	specific heat ratio
ω	vorticity
Ω	angular velocity
μ	dynamic viscosity
ρ	density
χ	chemical symbol

ACKNOWLEDGMENT

The work of OMK and ASW has been supported in part by the Office of Naval Research. HNN is supported the US Department of Energy, Office of Basic Energy Sciences, Chemical Sciences Division. Computations were performed at the Pittsburgh Supercomputer Center.

REFERENCES

1. Smooke, M.D., and Giovangigli, V. *Twenty Fourth Symposium (International) on Combustion*, The Combustion Institute, 1992, pp. 161-168.
2. Tien, J.H., and Matalon, M., *Combust. Sci. and Tech.* **87**:257-273 (1993).
3. Chen, R.H., Dirscoll, J.F., Kelly, J, Namazian, M., and Schefer, R.W., *Combust. Sci. and Tech.* **71**:197-217 (1990).
4. Tamir, A., *Combust. Sci. and Tech.* 90:193-209 (1993).
5. Chen, J.-Y., Mann, A.P., and Kent, J.H., *Twenty-Fourth Symposium (International) on Combustion*, The Combustion Institute, 1992, pp. 1381-1389.
6. Wang, H.Y., McDonell, V.G., and Samuelsen, G.S., *Twenty-Fourth Symposium (International) on Combustion*, The Combustion Institute, 1992, p. 1457-1463.
7. Hartley, L.J., and Dold, J.W., *Combust. Sci. and Tech.* **80**: 23-46 (1991).
8. Knio, O.M., Shi, X., and Ghoniem, A.F., "Lagrangian simulation of a thin non-premixed flame in the field of an asymmetric layer," *Comb. Flame* (in press).
9. Majda, A., and Sethian, J.A., *Comb. Sci. Tech* **42**: 185-205 (1987).
10. Ghoniem, A.F., *Lectures Appl. Math.* **24**: 199-265 (1986).
11. Najm, H.N., "A Conservative Low-Mach-Number Projection Method for Reacting Flow Modeling," in *Transport Phenomena in Combustion* (in press).
12. Daube, O., *J. Comput. Phys.* **103**:402-414, (1992).
13. Panton, R.L., *Incompressible Flow*, Wiley, New York, 1984.
14. Williams, F.A., *Combustion Theory*, Addison-Wesley, New York, 1985.

FIGURE CAPTIONS

Figure 1. Schematic illustration of the flow geometry; initial and boundary conditions are also indicated.

Figure 2. Evolution for the mixed-fraction index, PM.

Figure 3. Evolution of the "one-dimensional" structure of a premixed flame with $Da = 10000$, as depicted using radial profiles of: (a) the fuel burning rate, and (b) the temperature.

Figure 4. Fuel burning rate contours for $Da = 10000$ and $t_{ig} = 0$; (a) $t = \pi$, (b) $t = 4\pi$, (c) $t = 5\pi$, (d) $t = 6\pi$.

Figure 5. Reaction structure at $t = 6\pi$ for $Da = 10000$ and $t_{ig} = 0$, depicted using contours of (a) product concentration, (b) vorticity, (c) fuel concentration, and (d) oxidizer concentration.

Figure 6. Evolution of the thermodynamic pressure (top) and the burnt fraction (bottom) for $Da = 5000$ (a,c) and $Da = 10000$ (b,d). For each frame, curves are generated for $PM = 8.5\%$, $PM = 50\%$, and $PM = 90\%$. Results for the well-remixed case ($PM = 100\%$) are also plotted. In these plots, time is measured from the moment the mixture is sparked.

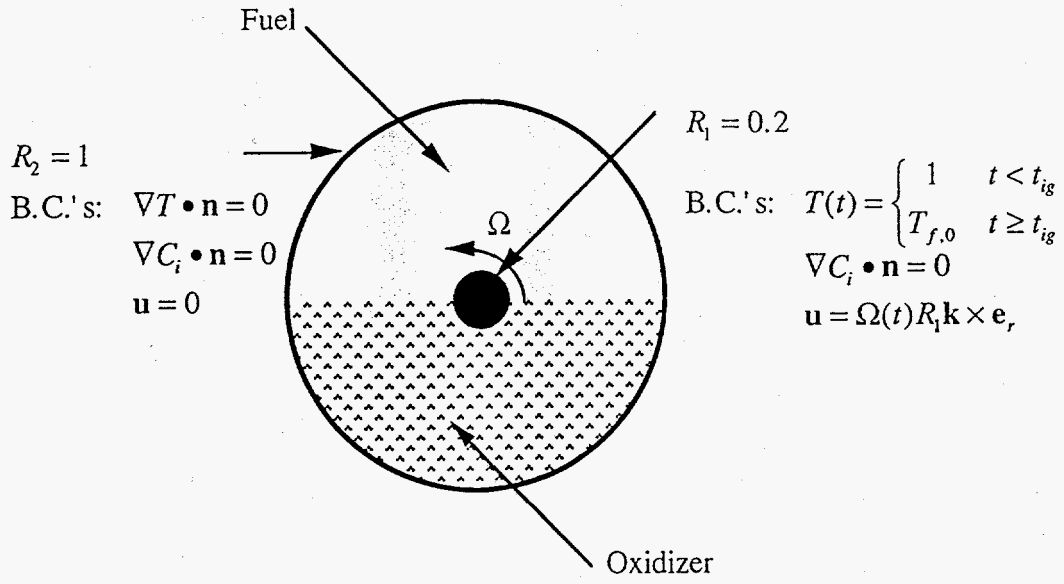
Fuel
$R_2 = 1$
B.C.'s: $\nabla T \bullet \mathbf{n} = 0$
$\nabla C_i \bullet \mathbf{n} = 0$
$\mathbf{u} = 0$
$R_1 = 0.2$
B.C.'s: $T(t) = \begin{cases} 1 & t < t_{ig} \\ T_{f,0} & t \geq t_{ig} \end{cases}$
$\nabla C_i \bullet \mathbf{n} = 0$
$\mathbf{u} = \Omega(t) R_1 \mathbf{k} \times \mathbf{e}_r$
Ω
Oxidizer

Figure 1

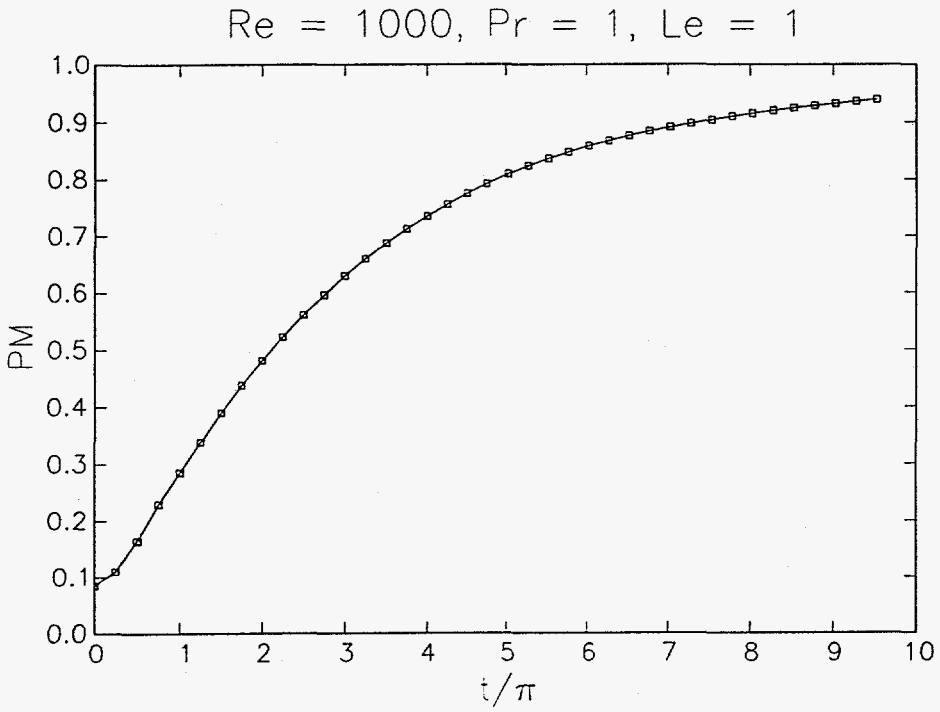
Re = 1000, Pr = 1, Le = 1
PM
1.0
0.9
0.8
0.7
0.6
0.5
0.4
0.3
0.2
0.1
0.0
0
1
2
3
4
5
6
7
8
9
10
t/π

Figure 2

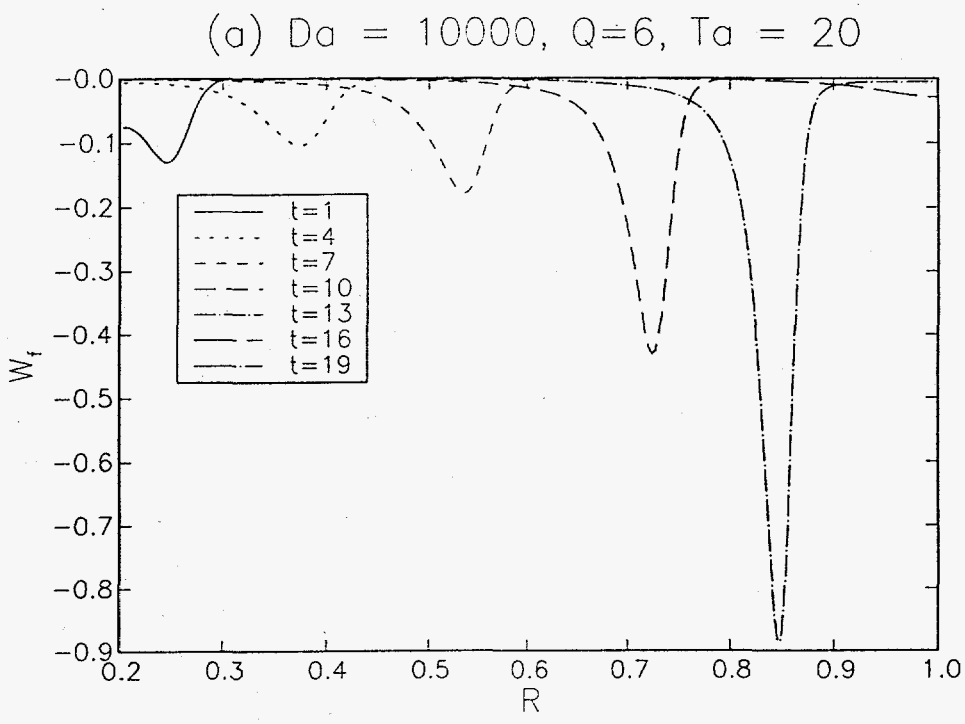
(a) Da = 10000, Q=6, Ta = 20
W_f
R
t=1
t=4
t=7
t=10
t=13
t=16
t=19

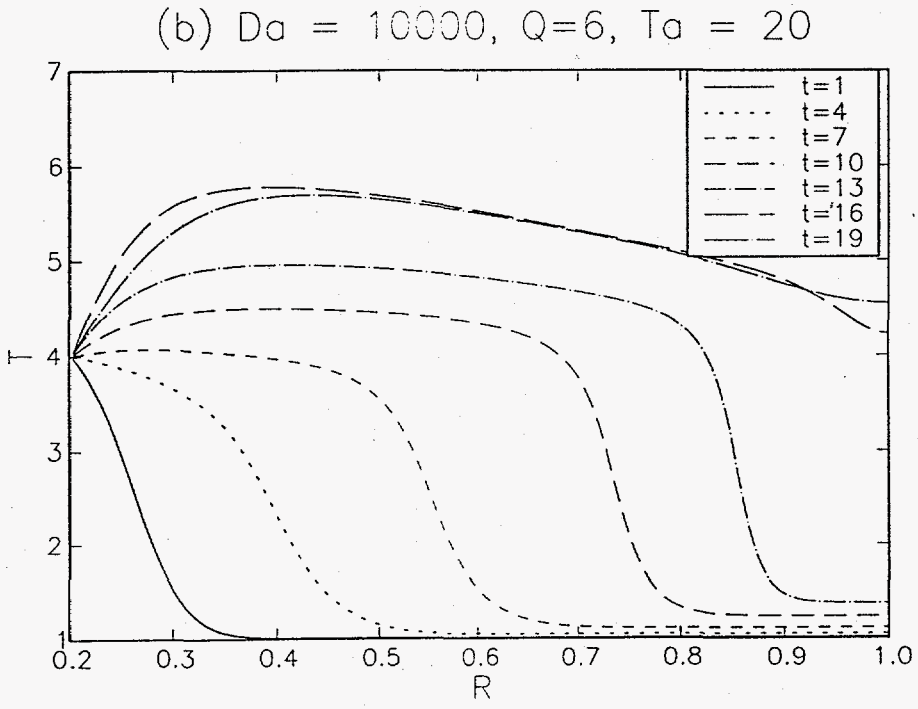
(b) Da = 10000, Q=6, Ta = 20
T
R
t=1
t=4
t=7
t=10
t=13
t=16
t=19

Figure 3

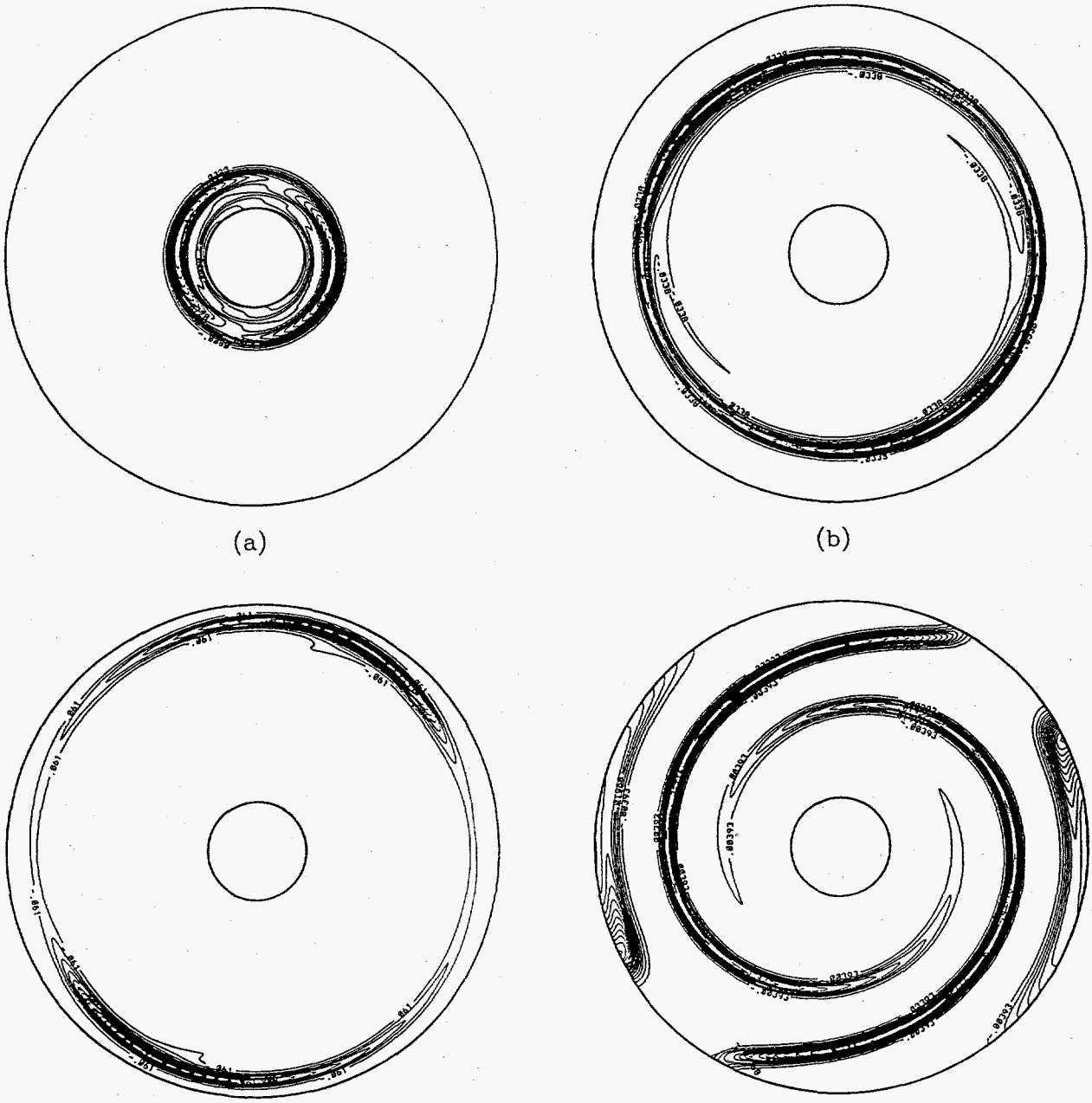

(a) (b)

(c) (d)

Figure 4

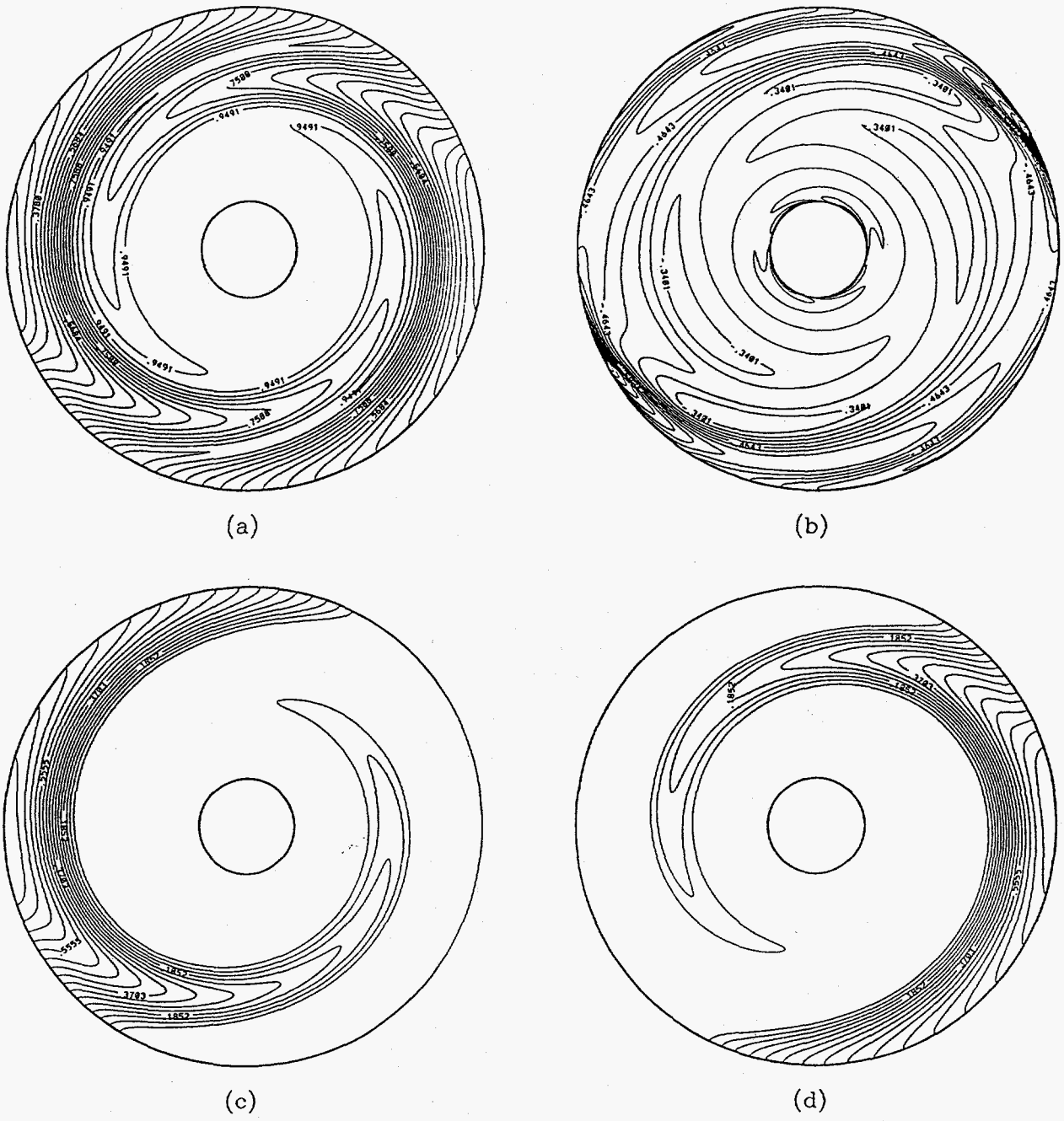

(a) (b)

(c) (d)

Figure 5

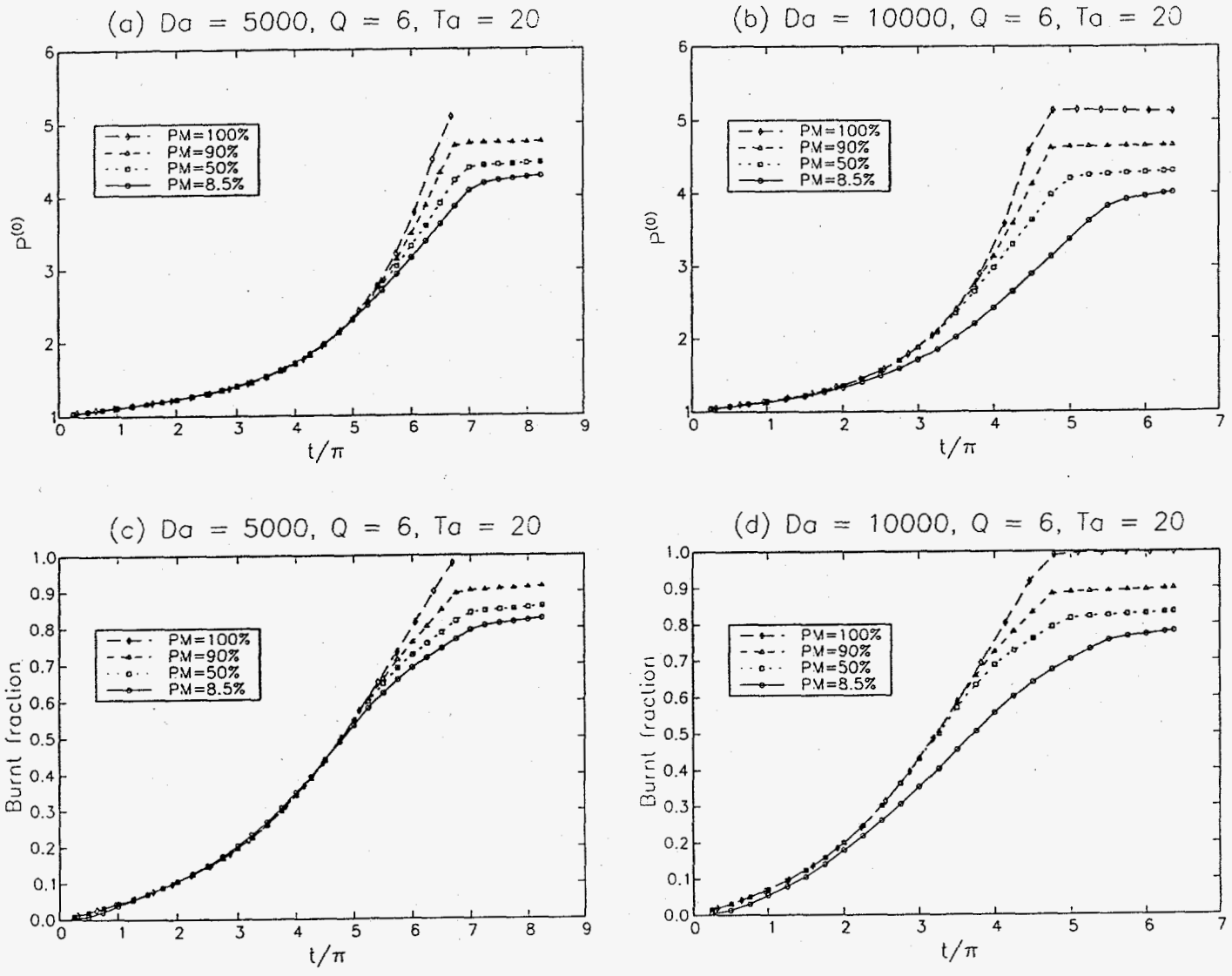
(a) Da = 5000, Q = 6, Ta = 20
(b) Da = 10000, Q = 6, Ta = 20
(c) Da = 5000, Q = 6, Ta = 20
(d) Da = 10000, Q = 6, Ta = 20
PM=100%
PM=90%
PM=50%
PM=8.5%
p(0)
Burnt fraction
t/π

Figure 6